15th IFK
Proc. of the 15th International Fluid Power Conference <Symposium/Conference>
<DOI>

Thermal-fluid coupling analysis of the Deflector Jet Servo Valve: effects of internal air region, oil viscosity, and coil heat source

Junhao Chen, Junru Hui, Mingjie Li*, Xiaoping Ouyang*

State Key Laboratory of Fluid Power and Mechatronic Systems, Zhejiang University, Hangzhou 310030, China

**Corresponding author: E-mail address: mingjielee@zju.edu.cn, ouyangxp@zju.edu.cn*

Abstract.

The thermal behavior of the deflector jet servo valve (DJSV) is influenced by complex interactions among electromagnetic, fluid, and thermal fields, making accurate temperature prediction challenging under wide operating conditions. However, most existing simulations rely on simplified assumptions (such as omitting the internal air region, assuming constant oil viscosity, or ignoring the coil heat source) without quantitatively assessing their effects on the predicted thermal field. In this study, a three-dimensional steady-state thermal-fluid coupled model of a DJSV is developed to evaluate the influence of these modeling simplifications. Six simulation schemes are designed by varying the treatment of the internal air domain, oil viscosity-temperature dependence, and coil heat generation, and are assessed under six representative operating conditions covering combinations of inlet oil temperature, ambient temperature, and pressure. Results show that omitting the internal air region mainly affects electromagnetic components, while neglecting temperature-dependent oil viscosity and coil heating causes distributed deviations across multiple parts. The coil and armature exhibit the highest thermal sensitivity. These findings clarify the thermal implications of modeling simplifications and provide reference for selecting appropriate model fidelity in engineering-oriented DJSV analyses.

Keywords. Deflector jet servo valve, thermal-fluid coupling, temperature field prediction, temperature dependence

1. INTRODUCTION

As a core component of electro-hydraulic servo control systems, the deflector jet servo valve (DJSV) critically determines system precision and reliability. In aerospace applications, hydraulic oil temperatures can vary widely, from below -50 °C to above 120 °C, and may even exceed 200 °C in high-performance systems. Excessive temperature rise can lead to severe consequences, such as spool jamming and degradation of electromagnetic components. Therefore, accurate prediction of the temperature field is essential for effective thermal management and reliable system design.

Numerous studies have investigated thermal effects in servo valves. Li et al. [1] developed a thermodynamic model that takes throttling losses and convective heat exchange into account and has been experimentally validated. Zhang et al. [2] applied a heat-fluid-solid FEM and found that thermal deformation of the spool-sleeve pair reduced the clearance and caused clamping above 80 °C. The zero-drift model in [3] attributed over 15 % control error (20-270 °C) to variations in flow coefficient and magnetic reluctance. An AMESim-based model [4] demonstrated that temperature reached equilibrium within 2.5 hours, with pressure having a strong influence. Recent efforts have focused on DJSVs. A nonlinear ninth-order model [5] demonstrated that temperature-induced flow-coefficient variation and pilot-stage deformation jointly degrade accuracy by over 30 %. Temperature-dependent flow-force evolution was quantified in [6], and wide-temperature modeling [7] linked magnetic-flux loss and air-gap deflection to temperature drift. Other studies [8-12] linked thermal friction and clearance reduction to jamming, demonstrated that reduced viscosity enhances self-excited oscillations, and clarified the leakage-clamping trade-offs at elevated temperatures. Collectively, these works confirmed that oil temperature significantly affects valve dynamics and stability.

However, most existing thermal analyses emphasize the hydraulic stage while neglecting the torque motor and its internal air region. The internal air region is often omitted or solidified, overlooking its role in convective heat transfer. Moreover, many models are confined to zero-opening conditions, where oil flow and heat convection are minimal, and oil viscosity is treated as constant rather than temperature-dependent. Such simplifications limit the accuracy of temperature-field prediction, particularly for electromagnetic components under realistic operating states. To address these limitations, this study establishes a three-dimensional steady-state thermal-fluid coupled model of a DJSV. Six simulation schemes with different simplifications, regarding the internal air region, oil-viscosity-temperature dependence, and coil heat generation, are evaluated under representative conditions to quantify their respective effects and clarify component-level thermal sensitivities.

2. THERMAL GENERATION AND HEAT TRANSFER IN DJSV

2.1. Operating Principle

The DJSV mainly consists of three functional subsystems: a torque motor, a jet prestage, and a power spool stage. The feedback rod passes through a pair of high-pressure jets and receiver ports on the jet pan, with V-shaped grooves machined on its surface. When an electric current flows through the coils, electromagnetic torque is generated in the magnetic circuit, producing a small angular deflection of the armature assembly. This deflection causes a displacement of the V-groove, which changes the pressure difference between the two receiver ports and consequently drives the spool motion in the power stage. During this energy conversion process, multiple heat generation and dissipation phenomena occur simultaneously. These include Joule heating within the coils, iron losses in the magnetic conductors, and throttling-induced viscous dissipation within the valve body. The generated heat is dissipated through several mechanisms: heat conduction, forced convection through hydraulic oil flow, and natural convection from the external surfaces of the valve to the surrounding air.

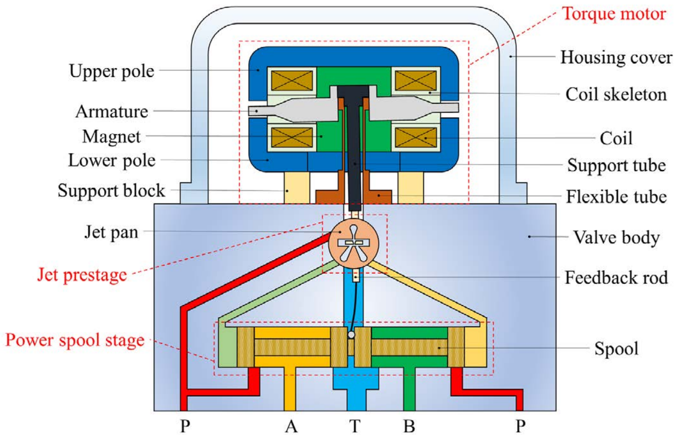

Figure 2.1. Structure of the deflector jet servo valve.

2.2. Heat Generation

(a) Electromagnetic Losses

When an electric current I passes through the coil, Joule heating occurs, with the instantaneous power expressed as:

$$P_{cu}=I^2R \tag{1}$$

The resistance of the coil varies with temperature according to:

$$R=R_0[1+\alpha(T\text{-}T_0)] \tag{2}$$

where R_0 is the resistance at the reference temperature T_0, and α is the temperature coefficient of resistivity. Assuming uniform current density and homogeneous heating, the winding region is treated as a uniformly distributed volumetric heat source. The volumetric heat generation rate is then expressed as:

$$q_{\mathrm{cu}}=\frac{I^2R}{V} \tag{3}$$

where V is the coil volume.

The present model neglects dynamic magnetic losses (iron losses) but incorporates the temperature-dependent copper loss to account for the resistivity-temperature coupling in the windings.

(b) Throttling-Induced Heat Generation

Viscous dissipation during throttling arises from viscosity-induced energy losses. As hydraulic oil flows through the orifice, the abrupt reduction in flow area accelerates the fluid and produces a high shear rate. Viscous stresses resist the velocity gradient, converting flow work and turbulent kinetic energy into internal energy and heat. The resulting temperature rise inside the valve due to viscous dissipation is given by:

$$\Delta T=\frac{\Phi}{\rho c_{\mathrm{p}}} \tag{4}$$

where ρ is the oil density, c_p is the specific heat at constant pressure, and Φ is the viscous dissipation function:

$$\Phi=\mu\{2[\left(\frac{\partial u}{\partial x}\right)^2+\left(\frac{\partial v}{\partial y}\right)^2+\left(\frac{\partial w}{\partial z}\right)^2]+\left(\frac{\partial u}{\partial y}+\frac{\partial v}{\partial x}\right)^2+\left(\frac{\partial u}{\partial z}+\frac{\partial w}{\partial x}\right)^2+\left(\frac{\partial v}{\partial z}+\frac{\partial w}{\partial y}\right)^2\} \tag{5}$$

where μ is the fluid dynamic viscosity, u, v, w are the velocity components of the fluid in the x, y, z directions. The dynamic viscosity is treated as temperature-dependent, according to the fitted viscosity-temperature relation in Section 3.2.

2.3. Heat Transfer

(a) Forced Convection

Within the valve body, hydraulic oil flow driven by the pressure differential transfers heat away from internal components. The convective heat flux can be expressed by Newton's law of cooling:

$$q=h(T_w-T_f) \tag{6}$$

where h is the convective heat transfer coefficient, T_w is the wall temperature, and T_f is the fluid bulk temperature. The coefficient h can be estimated using a Nusselt number correlation of the form:

$$N_u=\frac{hL_c}{\lambda}=CR_e^m P_r^n \tag{7}$$

where L_c is the characteristic length, λ is the thermal conductivity, R_e is the Reynolds number, P_r is the Prandtl number, C, m, n are the empirical coefficients. The dynamic viscosity of the hydraulic oil varies exponentially with temperature and is described by:

$$\mu(T)=\mu_0 e^{-b(T-T_0)} \tag{8}$$

where μ_0 is the viscosity at the reference temperature T_0, and b is the empirical constant.

(b) Natural Convection

Heat dissipation from the external surfaces of the valve to ambient air occurs primarily via natural convection, which can be described as:

$$q=h_{nat}(T_s-T_\infty) \tag{9}$$

where h_{nat} is the natural convection coefficient, T_s is the surface temperature, and T_∞ is the ambient air temperature.

(c) Heat Conduction and Internal Air Domain

Heat conduction follows the Fourier's law:

$$q=-k\nabla T \tag{10}$$

where k is the thermal conductivity, ∇T is the temperature gradient vector.

Within the enclosed housing, natural convection is limited, allowing the air to be approximated as a solid with low thermal conductivity.

3. Numerical Simulation Model and Methodology

3.1. Modeling Overview and Meshing strategy

The model preprocessing of the DJSV is shown in **Figure 3.1**, ignoring non functional details such as chamfers, screw holes, and fillets. Assuming an input current of 40 mA, the corresponding displacement of the spool valve is set to -0.5 mm, and the displacement of the jet prestage deflection is set to +0.025 mm. Consequently, the computed temperature field reflects a quasi-steady-state thermal balance at a representative operating point.

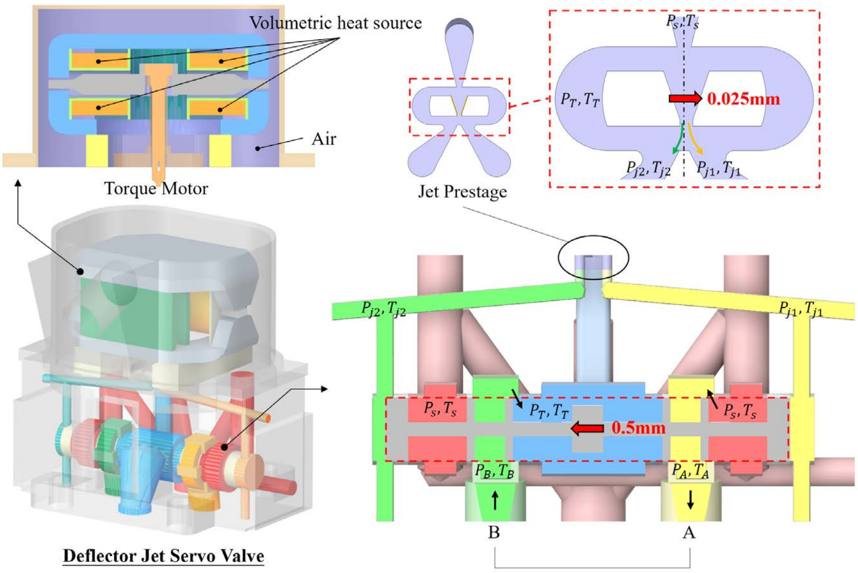

Figure 3.1. Model preprocessing of the DJSV

The mesh generation result for the entire valve is shown in **Figure 3.2**. Local refinement was applied to the orifices of the jet pilot stage and the spool, and the total number of grid cells reached 2 million.

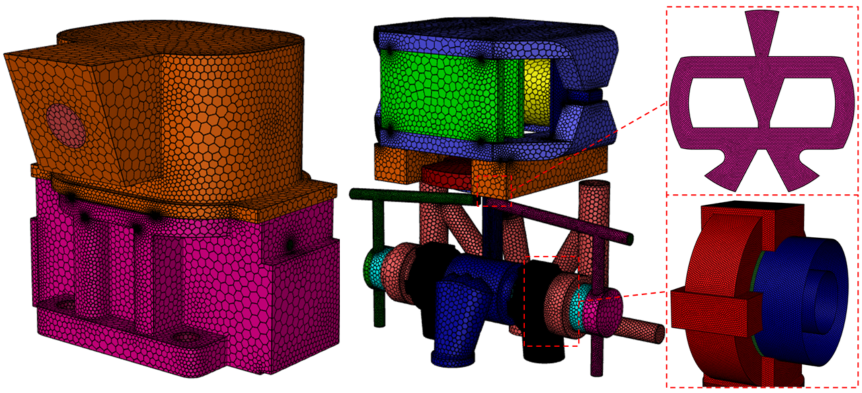

Figure 3.2. Mesh generation and local refinement

The velocity contour results in **Figure 3.3** confirm that the mesh adequately resolves the flow structures and velocity gradients within the critical regions, including the jet prestage and throttling orifice.

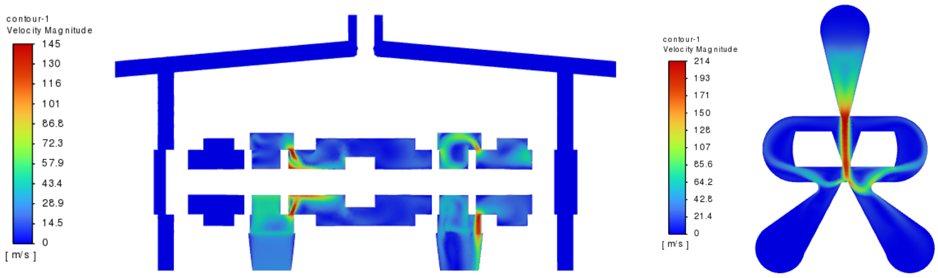

(a)valve body section (b) jet prestage section

Figure 3.3. Representative velocity contour results

3.2. Material Properties

The thermal physical properties are summarized in **Table 1**. The component "Solid-air" is the equivalent solid region.

Table 1: Materials settings

Component	Material	Density (kg/m^3)	Specific heat capacity (J/(kg·K))	Thermal conductivity (W/(m·K))
Housing cover Support block	0Cr18Ni9	7930	500	21.5
Upper pole Lower pole Armature	1J50	8100	460	15
Magnet	LNG32	7500	465	32.7
Support tube Feedback rod	3J1	8100	460	30
Flexible tube	Qbe2	8300	380	100
Spool	9Cr18	7700	470	29.3
Valve body	440C	7800	480	24.2
Coil	Copper	8930	385	390
Coil skeleton	Polyimide	1400	1150	0.25
Solid-air	-	1.205	1012	0.026
Oil	YH-15 aviation hydraulic oil	850	1880	0.12

The hydraulic medium is YH-15 aviation hydraulic oil, the temperature dependence of the oil viscosity was obtained from experimental data (see **Table 2**). A double-exponential correlation derived by least-squares fitting (R^2=0.99996) is expressed as:

$$\mu(\mathrm{T})=0.0017e^{-0.1182T}+0.0389e^{-0.0312T} \tag{11}$$

where $\mu(\mathrm{T})$ is the viscosity of the oil (kg/(m·s)), T is the temperature of the oil (°C).

Table 2: Viscosity test results of YH-15 aviation hydraulic oil [13]

Temperature/℃	Viscosity/(mm^2/s)	Temperature/℃	Viscosity/(mm^2/s)
-55	1620.993	60	9.683
-40	390.924	80	7.088
-20	111.064	100	5.579
0	42.734	120	4.460
20	22.482	135	4.027
40	13.928		

3.3. Boundary Conditions and Simulation Settings

The energy equation with viscous dissipation was activated, and the Realizable k-epsilon model was employed as the turbulence model. The boundary condition settings are as follows:

Table 3: Boundary condition settings

Boundary Location	Type	Parameter	Value
Port P	Pressure inlet	pressure temperature	**inlet_pressure** **inlet_temp**
Port A	Pressure outlet	pressure	(**inlet_pressure**+0.5MPa)/2
Port B	Pressure inlet	pressure temperature	(**inlet_pressure**+0.5MPa)/2 Outlet A temperature
Port T	Pressure outlet	pressure	0.5 MPa
Outer surfaces	Convection	temperature coefficient	**ambient_temp** 10 W/(m²·K)

All solid-fluid and solid-solid interfaces employed shared topology to ensure continuous heat flux. The temperature-dependent volumetric heat source of the coil was expressed as:

$$q_{\mathrm{v}}(T)=(I^2\cdot\frac{234+T}{254}\cdot R_{20})/V=160000\cdot\frac{234+T}{254} \tag{12}$$

where $q_{\mathrm{v}}(T)$ is the volumetric heat power (W/m^3), T is the temperature of coil (℃), I is the current (A), R_{20} is the resistance of the coil at 20℃ (Ω), V is the coil volume (m^3).

Table 4: Multiple operating conditions

Condition	**ambient_temp**/℃	**inlet_pressure**/MPa	**inlet_temp**/℃
C1	25	21	25
C2	25	35	25
C3	300	21	25
C4	25	21	135
C5	25	35	135
C6	300	21	135

As shown in **Table 4**, the boundary conditions cover six representative operating environments (C1-C6) to evaluate the modeling assumptions under normal, high-pressure, and high-temperature conditions. Case C3 (300 °C ambient, 25 °C inlet oil) reflects hot external exposure with a relatively low inlet-oil temperature, creating a high-ambient and low-supply contrast to quantify the oil-cooling effect and the resulting temperature gradients. To systematically assess the influence of modeling assumptions, six simulation schemes (S1-S6) were constructed as shown in **Table 5**. Each scheme isolates one or more simplifications related to the internal air region, oil viscosity–temperature dependence, and coil heat-source modeling. Scheme S1 serves as the reference model, while S2-S6 progressively omit selected coupling effects.

Table 5: Summary of simulation schemes

Scheme	Air region treatment	Viscosity model	Coil heat source
S1	Equivalent solid	Variable $\mu(T)$	Variable $q_v(T)$
S2	Equivalent solid	Constant μ	Constant q_v
S3	Equivalent solid	Constant μ	Ignored
S4	Ignored	Variable $\mu(T)$	Variable $q_v(T)$
S5	Ignored	Constant μ	Constant q_v
S6	Ignored	Constant μ	Ignored

4. SIMULATION RESULTS AND DISCUSSION

4.1. Overall Temperature Distribution under Typical Condition

To intuitively demonstrate the influence of model simplification on thermal field prediction, the temperature distributions obtained from the most detailed scheme (S1) and the most simplified scheme (S6) were compared under two representative operating conditions: C1 and C6. These two cases correspond to the normal and high-temperature extremes, enabling a direct comparison of the valve's thermal behavior under ordinary and harsh environments.

As shown in **Figure 4.1**, under the normal temperature condition, the overall temperature gradient across the valve is relatively small. The high temperature zones are mainly concentrated at the spool throttling orifice and the jet prestage, where viscous dissipation is strongest. A temperature gradient exists along the feedback rod within the torque motor, whereas the temperature distribution in the remaining components is relatively uniform.

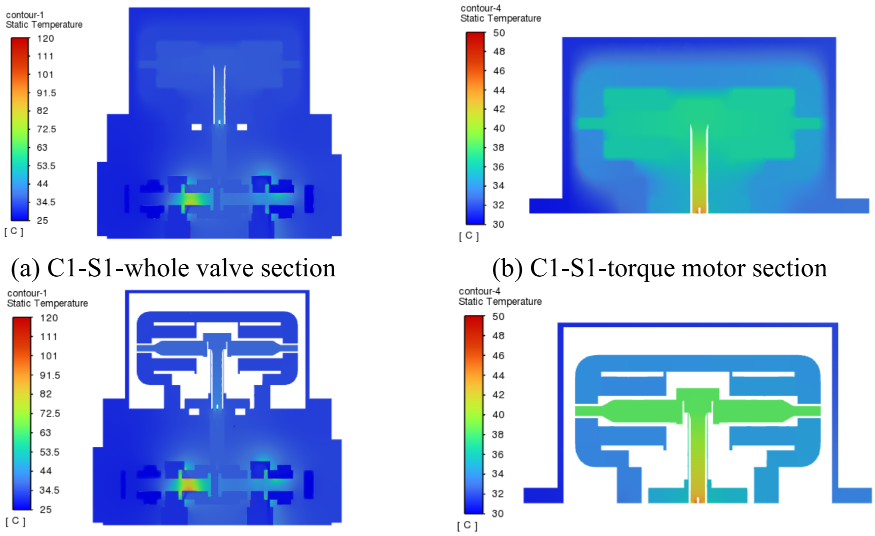

(a) C1-S1-whole valve section (b) C1-S1-torque motor section

(c) C1-S6-whole valve section (d) C1-S6-torque motor section

Figure 4.1. Temperature contours under C1 between S1 and S6

As shown in **Figure 4.2**, under the high temperature condition, however, the thermal gradient becomes much more pronounced. The highest temperature occurs at the top of the housing cover, while the return oil region in the valve body is also relatively hot.

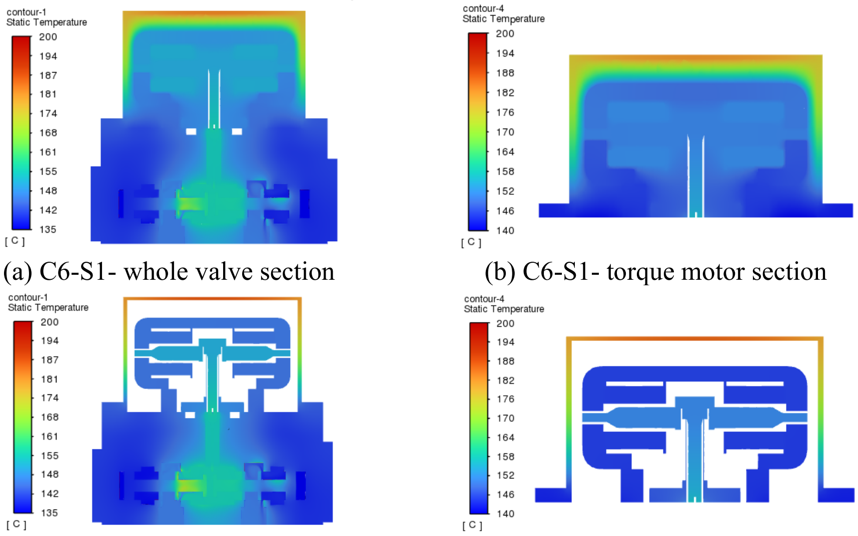

(a) C6-S1- whole valve section (b) C6-S1- torque motor section

(c) C6-S6- whole valve section (d) C6-S6- torque motor section

Figure 4.2. Temperature contours under C6 between S1 and S6

When comparing S1 and S6, the global temperature distributions of the valve appear similar under both C1 and C6, suggesting that at a macroscopic level the main heat-transfer paths and primary hot zones are preserved in the simplified model. Nevertheless, the torque motor cross section reveals localized discrepancies between the two schemes. To assess these deviations, a quantitative comparison of component-level temperatures is presented in the next section.

4.2. Deviation Analysis of Different Modeling Schemes

Twelve structural components of the DJSV were defined as monitoring bodies for thermal evaluation, as listed below: (1) armature, (2) coil, (3) housing cover, (4) support block, (5) feedback rod, (6) flexible tube, (7) lower pole, (8) magnet, (9) spool, (10) support tube, (11) upper pole, and (12) valve body. The volume averaged steady-state temperature of each component was extracted under all modeling schemes (S1-S6) and operating conditions (C1-C6) for quantitative comparison.

Figure 4.3 presents the relative temperature deviations of twelve components under six operating conditions (C1-C6). Under the conventional condition C1, temperature deviations mainly occurred in the armature, coil, spool, and support tube. When the pressure increased (C1→C2), The deviations of the armature and support tube became larger, while other components remained nearly unchanged. During ambient temperature elevation (C1→C3), a wider range of components showed pronounced changes. The deviations of the armature, coil, magnet, and both magnetic poles shifted significantly, with several instances of sign reversal and magnitudes up to 10-12%. However, under high-temperature oil conditions, the transitions C4→C5 and C4→C6 produced negligible changes. When comparing oil temperature increase pairs (C1→C4, C2→C5, C3→C6), several components demonstrated evident deviations. For example, the armature and support tube showed large variations in C2→C5 (-8%), while in C3→C6 the coil, magnet, and upper pole exhibited positive deviations up to 9%.

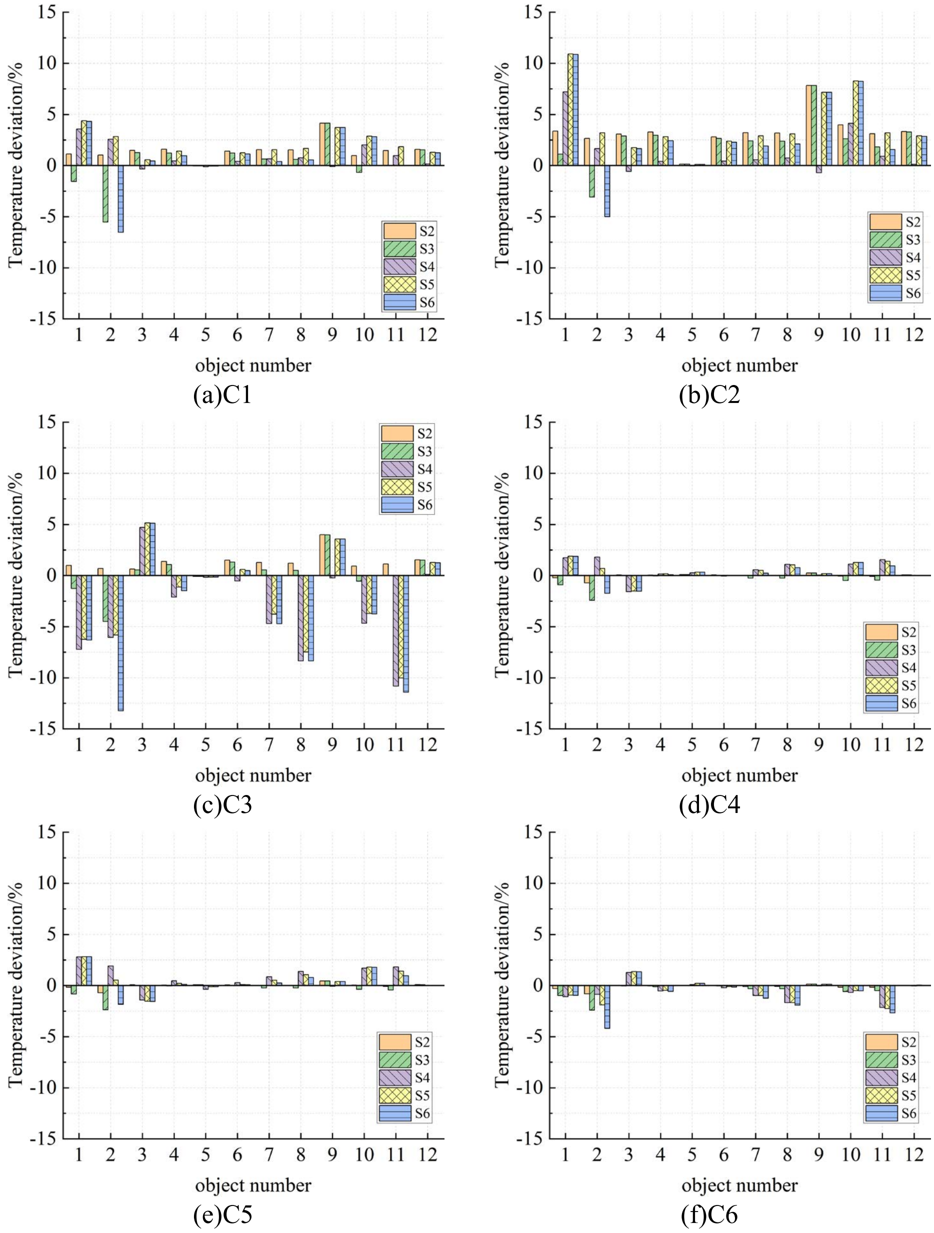

1-armature; 2-coil; 3-housing cover; 4-support block; 5-feedback rod; 6-flexible tube; 7-lower pole; 8-magnet; 9-spool; 10-support tube; 11-upper pole; 12-valve body

Figure 4.3. Bar charts of temperature deviations relative to S1 under condition C1-C6

4.3. Average Absolute Deviation and Sensitivity Evaluation

To further quantify the global influence of model simplifications, the average absolute deviation (AAD) of the twelve components was calculated for each scheme under all six operating conditions, as shown in **Figure 4.4**. The AAD provides a single comprehensive metric representing the overall discrepancy introduced by each modeling assumption.

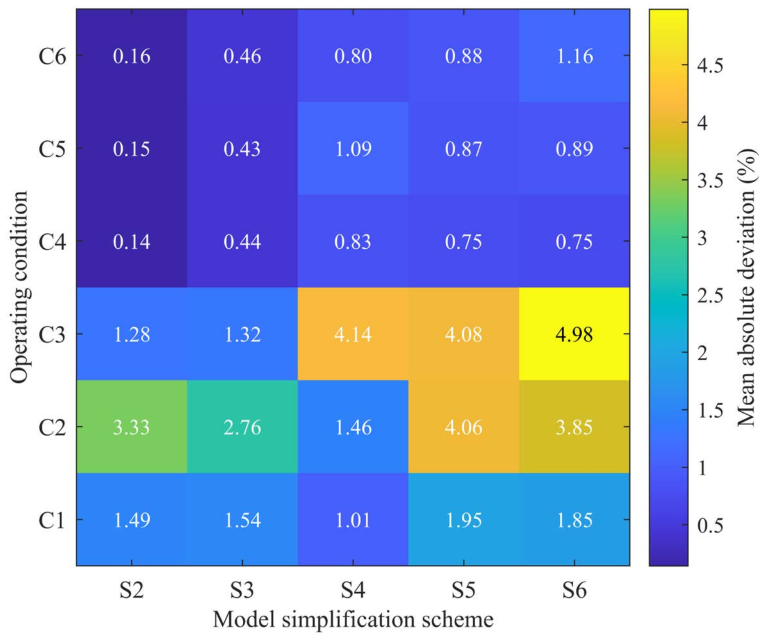

Figure 4.4. Heatmap of average absolute deviation under C1-C6

Under high oil inlet temperatures (C4-C6), the AAD values of all simplified schemes remain relatively low, suggesting that the convective heat transfer of the hot oil plays a primary role in shaping the valve's overall thermal response. In this regime, the temperature viscosity dependence of the oil tends to stabilize, diminishing the impact of the assumed viscosity model on thermal dissipation. Therefore, neglecting the internal air domain and the temperature dependence of viscosity and coil resistance has a negligible impact on the overall error. In contrast, under moderate thermal conditions (C2 and C3), the deviation increases notably, particularly for the more simplified schemes (S4-S6), reaching up to about 5%. This indicates that, when the inlet oil temperature remains at room temperature while the ambient temperature intensifies, neglecting the internal air region removes an important thermal resistance path, thus introducing a discernible discrepancy in the predicted temperature field. Moreover, under high pressure conditions (C2 and C5), the intensified viscous dissipation in the throttling orifices elevates local temperatures, which may be inadequately represented if the temperature dependence of oil viscosity is ignored.

To isolate the influence of each modeling factor, including the omission of the internal air region, the neglect of temperature-dependent effects (for both viscosity and coil heat generation), and the complete omission of the coil heat source, pairwise comparisons were conducted such that only the factor of interest varied while the other two remained fixed.

The scheme pairings used for each isolated factor are summarized in **Table 6**. This approach ensures that the extracted deviations reflect the individual contribution of each simplification rather than the combined influence of multiple assumptions.

Table 6: Scheme pairs used for single-factor sensitivity analysis

Factor	Scheme Pair for Comparison
Omit air region	S4-S1, S5-S2, S6-S3
Temperature dependence(Viscosity/Coil heat source)	S2-S1, S3-S1, S5-S4, S6-S4
Ignore coil heat source	S3-S2, S6-S5

As shown in **Figure 4.5**, the coil consistently exhibits the highest temperature sensitivity, with deviations exceeding 1.6% for all factors and reaching up to 2.9% when the coil heat source is completely neglected. The armature demonstrates pronounced sensitivity primarily to the air-domain omission, with deviations up to 2.75%. When the temperature-dependent effects of viscosity and coil heating are ignored, deviations are moderate but widely distributed across multiple components, particularly the spool, support tube, and magnet, reflecting the system-wide influence of assuming constant material properties. In contrast, the valve body, flexible tube, and feedback rod exhibit minimal changes across all factors. Therefore, accurate inclusion of both the air domain and temperature dependent effects is essential for reliable prediction of local thermal gradients within the torque motor assembly.

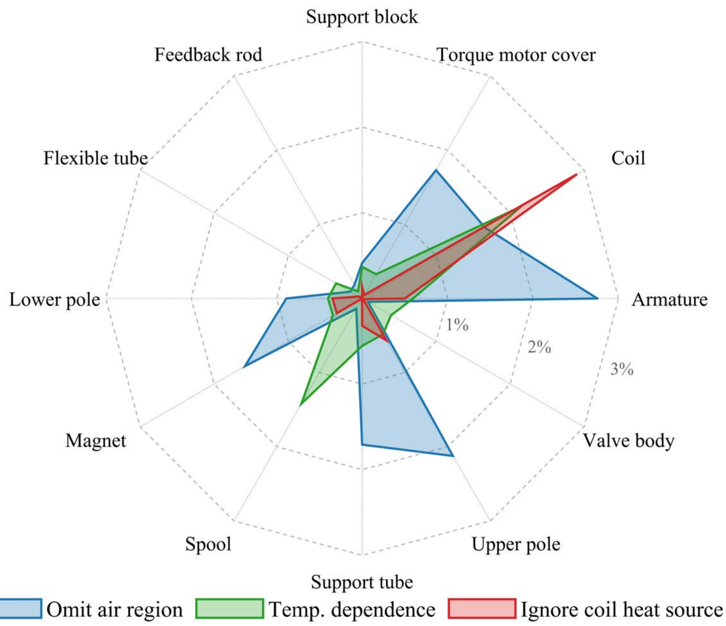

Figure 4.5. Sensitivity of component temperature deviation to modeling simplifications

5. CONCLUSIONS

A steady-state three-dimensional thermal-fluid coupled analysis of a deflector jet servo valve (DJSV) was performed. The analysis quantified the effects of common modeling simplifications, including the omission of the internal air domain, neglect of temperature-dependent oil viscosity and coil heat generation, and complete exclusion of the coil heat source. Six simulation schemes were examined under six representative operating conditions to evaluate the resulting thermal deviations. The results indicate that the simplified models generally preserve the primary heat-transfer paths and dominant hot zones. However, neglecting the internal air region primarily affects electromagnetic components, particularly under elevated ambient temperatures. Ignoring the temperature dependence of oil viscosity and coil heating introduces distributed temperature deviations across multiple components. Among all factors, the coil exhibits the highest sensitivity, the armature is mainly affected by the omission of the air region, while the spool, support tube, and magnet show moderate deviations when temperature-dependent effects are disregarded. In contrast, the valve body, flexible tube, and feedback rod remain largely insensitive to these simplifications.

Acknowledgement

This work was supported by the National Key Research and Development Program of China under Grant 2024YFF0505300, National Natural Science Foundation of China under Grant 52405078.

6. References

[1] Lei L, Gen W, Libo Q, Cunkun C. Research on thermodynamic modeling and temperature prediction of double flapper-nozzle servo valves. *Case Studies in Thermal Engineering*. 2024; 60: 104664. doi: 10.1016/j.csite.2024.104664.

[2] Zhao J, Zhou S, Lu X, et al. Numerical simulation and experimental study of heat-fluid-solid coupling of double flapper-nozzle servo valve. *Chinese Journal of Mechanical Engineering*. 2015; 28: 1030-1038. doi: 10.3901/CJME.2015.0417.045.

[3] Ma L, Yan H, Cai C, Ren Y. Mechanism of temperature-induced zero drift on electro-hydraulic servo valve. *AIP Advances*. 2021; 11: 065210. doi: 10.1063/5.0049045.

[4] Zhu Y, Zhang Q, Tao J, Tan D, Wang X. Heat characteristics analysis of electro-hydraulic servo valve. *Journal of Thermal Science and Engineering Applications*. 2019; 11(3): 031008. doi: 10.1115/1.4041880.

[5] Ma L, Yan H, Cai C, Ren Y. Temperature drift mechanism of deflector jet servo valve under temperature shock. *Proceedings of the Institution of Mechanical Engineers, Part I: Journal of Systems and Control Engineering*. 2022; 237(3): 462-478. doi: 10.1177/09596518221132457.

[6] Ma L, Liu Y, Wan L, Wang J, Yan H. Temperature characteristics of flow force in the pre-stage of deflector jet servo valve across a wide temperature range. *Case Studies in Thermal Engineering*. 2025; 74: 106967. doi: 10.1016/j.csite.2025.106967.

[7] Xiaoxue L, Yaobao Y, Shuwei Z, Tao J, Qiang X. The modeling and analysis of operating characteristics and temperature drift of deflector jet servo valve under the wide temperature range. *Proceedings of the Institution of Mechanical Engineers, Part C: Journal of Mechanical Engineering Science*. 2024; 238(12): 5921-5936. doi: 10.1177/09544062231219313.

[8] Zhang Y, Wang S, Shi J, Wang X. Evaluation of thermal effects on temperature-sensitive operating force of flow servo valve for fuel metering unit. *Chinese Journal of Aeronautics*. 2020; 33(6): 1812-1823. doi: 10.1016/j.cja.2019.09.011.

[9] Ma L, Yan H, Ren Y, Li L, Cai C. Numerical investigation of flow force and cavitation phenomenon in the pilot stage of electrical-hydraulic servo valve under temperature shock. *Machines*. 2022; 10(6): 423. doi: 10.3390/machines10060423.
[10] Chen Z, Wang W. Analysis of temperature characteristics of electro-hydraulic servo valve based on AMESim. In: *Proceedings of the 2018 International Conference on Mechanical, Electrical, Electronic Engineering and Science (MEEES 2018)*. Atlantis Press; 2018: 47-53. doi: 10.2991/meees-18.2018.10.
[11] Zhang X, Yin Y, Huang W. Influence of temperature on null position pressure characteristics of flapper-nozzle servo valve. In: *2010 International Conference on Computer Design and Applications (ICCDA)*. Qinhuangdao, China; 2010: V3-257-V3-261. doi: 10.1109/ICCDA.2010.5540780.
[12] Xu L, Ma H, Ren D. Numerical simulation for multi-way valves and fit clearance research based on heat-fluid-solid coupling. *The Journal of Engineering*. 2019; 2019(13): 247-252. doi: 10.1049/joe.2018.9036.
[13] Huang H, Mao Yang, Sun Yongbin, et al. Test and analysis of YH-15 aviation hydraulic oil viscosity-temperature characteristics. *Ordnance Industry Automation*. 2015, 34(05), 42-43. doi: 10.7690/bgzdh.2015.05.012.

Biographies

Junhao Chen received the bachelor's degree in mechanical engineering from Zhejiang University of Technology in 2023. He is currently working toward the Ph.D. degree in mechanical engineering with the State Key Laboratory of Fluid Power and Mechatronic Systems, Zhejiang University, Hangzhou, China. His research areas include multi-physics coupled modeling and reliability enhancement of servo valves.

Junru Hui received the bachelor's degree in energy and power engineering from Lanzhou University of Technology in 2019 and master's degree in mechanical engineering from The University of Sheffield in 2021. He is currently working toward the Ph.D. degree in mechanical engineering with the State Key Laboratory of Fluid Power and Mechatronic Systems, Zhejiang University, Hangzhou, China. His research areas include the internal performance changes of electro-hydraulic servo valves and the design of new configurations.

Mingjie Li received the bachelor's degree and Ph.D. degree in mechatronic engineering from Zhejiang University, Hangzhou, China, in 2013 and 2019. He is currently an assistant researcher in school of mechanical engineering, Zhejiang University. His research interests include control of electro-hydraulic systems and robotic systems.

Xiaoping Ouyang received the bachelor's degree and master's degree from Northeast Petroleum University Daqing, China, in 1997 and 2000, respectively, and the Ph.D. degree from Zhejiang University, Hangzhou, China, in 2005, all in mechanical engineering. He is currently a Professor with the State Key Laboratory of Fluid Power and Mechatronic Systems, and the Director with the Institute of Fluid Power and Intelligent Control, Zhejiang University. His research interests include electrohydraulic components and systems, and exoskeleton and humanoid robots.